

Threshold-free estimation of entropy from a Pearson matrix

H. Felipe^{1,2*}, A. Viol³, D.B. de Araujo⁴, M.G.E. da Luz⁵,

F. Palhano-Fontes⁴, H. Onias⁴, E.P. Raposo⁶, G.M. Viswanathan^{1,7}

¹ *Department of Physics, Federal University of Rio Grande do Norte - Natal-RN, 59078-970, Brazil*

² *Department of Network and Data Science, Central European University - Vienna, 1100, Austria*

³ *Cognitive Neuroscience, Scuola Internazionale Superiore di Studi Avanzati - Trieste, 34136, Italy*

⁴ *Brain Institute, Federal University of Rio Grande do Norte - Natal-RN, 59076-550, Brazil*

⁵ *Departamento de Física, Universidade Federal do Paraná - Curitiba-PR, 81531-980, Brazil*

⁶ *Laboratório de Física Teórica e Computacional, Departamento de Física, Universidade Federal de Pernambuco - Recife-PE, 50670-901, Brazil*

⁷ *National Institute of Science and Technology of Complex Systems, Federal University of Rio Grande do Norte - Natal-RN, 59078-970, Brazil*

(Dated: February 7, 2023)

There is demand in diverse fields for a reliable method of estimating the entropy associated with correlations. The estimation of a unique entropy directly from the Pearson correlation matrix has remained an open problem for more than half a century. All existing approaches lack generality insofar as they require thresholding choices that arbitrarily remove possibly important information. Here we propose an objective procedure for directly estimating a unique entropy of a general Pearson matrix. We show that upon rescaling the Pearson matrix satisfies all necessary conditions for an analog of the von Neumann entropy to be well defined. No thresholding is required. We demonstrate the method by estimating the entropy from neuroimaging time series of the human brain under the influence of a psychedelic.

An important open problem in many fields concerns how to estimate the entropy from the Pearson correlation matrix of an arbitrary data set [1–3]. This problem has wide and immediate applicability to diverse phenomena, *e.g.*, correlated asset prices [4, 5], diffusion processes [6], and brain networks [7–9]. The Shannon entropy solves the simpler problem of how to calculate the entropy given a probability distribution [10]. However, attempts to extend this formalism to estimate the entropy of a correlation matrix have required admittedly ad hoc methods, such as the thresholding of the correlation matrix to generate a new symmetric and unweighted adjacency matrix consisting only of 0’s and 1’s [11, 12]. The resulting adjacency matrix represents a simple graph, which can then be studied using topological metrics. These methods have led to significant advances in diverse fields, examples of which include applications to market volatility in financial crisis [13], and to scale-free and small-world brain networks [14–16]. Nevertheless, they have drawbacks that motivate the search for better approaches [17].

The main limitation of the existing methods is that the thresholding operation inevitably leads to loss of information [18]. Consider, for example, the set of all possible 2×2 Pearson correlation matrices. Since a correlation coefficient can assume any real value in the closed interval $[-1, 1]$, there are an infinite number of possible 2×2 Pearson matrices. In contrast, there are only two corresponding adjacency matrices of size 2×2 because a simple graph with two nodes is either

connected or disconnected. Significant information can thus be lost due to thresholding. As an important example, we mention that in neuroimaging data the results are not always robust with respect to the choice of thresholding [19, 20]. Insofar as unweighted matrices are used, these methods are only indirectly measuring the entropy of correlations, generally via topological metrics such as network motifs [21], degree distribution [22], and geodesic diversity [23]. There is thus a growing and vexing demand for a better method of estimating entropy.

Here, we demonstrate that the problem of how to calculate the entropy of a correlation matrix can be solved without the need of an adjacency matrix or ad hoc schemes. Let \mathbf{R} be a general $N \times N$ Pearson correlation matrix and let $\boldsymbol{\rho} = \mathbf{R}/N$. We show below that $\boldsymbol{\rho}$ has N non-negative eigenvalues λ_j that add up to 1, so that $\boldsymbol{\rho}$ has unit trace (*i.e.*, $\text{tr}\boldsymbol{\rho} = 1$). If we interpret these eigenvalues as a probability distribution, then we can define the Shannon entropy for this distribution according to

$$S(\boldsymbol{\rho}) = - \sum_{j=1}^N \lambda_j \log \lambda_j . \quad (1)$$

In terms of the trace of a matrix, we can equivalently write the above as

$$S(\boldsymbol{\rho}) = -\text{tr}(\boldsymbol{\rho} \log \boldsymbol{\rho}) . \quad (2)$$

The reader familiar with quantum statistical mechanics will immediately recognize Eq. (2) as an analogue of the von Neumann entropy for a density operator $\boldsymbol{\rho}$ for an ensemble of states with probabilities λ_j [24]. Indeed, the problem of calculating the entropy

* Corresponding author: h.felippe@fisica.ufrn.br

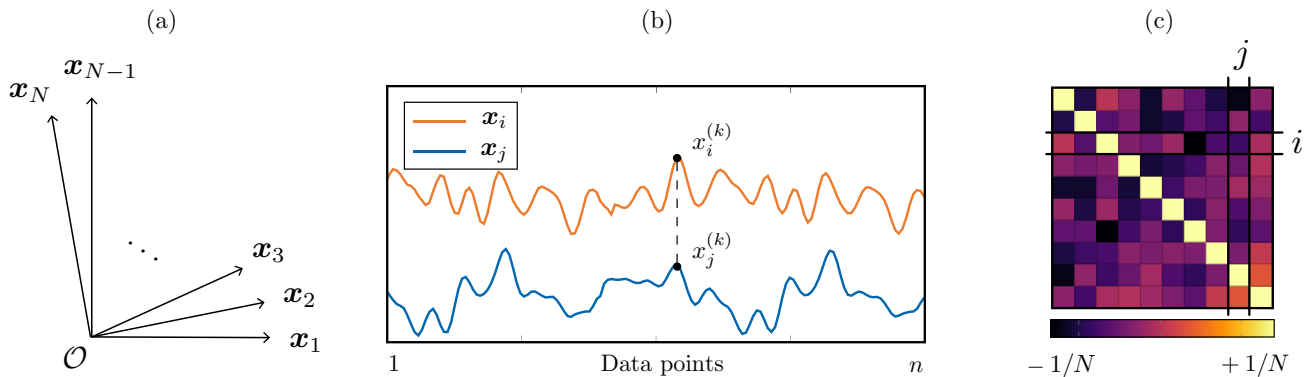


Figure 1. The construction of a density matrix from a Pearson correlation matrix. (a) The system of interest is partitioned into N interacting components or nodes. (b) The correlation between nodes i and j is then calculated. For each i node there are n data points $x_i^{(k)}$ where $k = 1, \dots, n$. The correlation R_{ij} between nodes i and j is given by Eq. (3), and lies in the interval $-1 \leq R_{ij} \leq 1$. (c) For each correlation coefficient R_{ij} , we calculate $\rho_{ij} = R_{ij}/N$, yielding the matrix $\rho = \mathbf{R}/N$. This matrix ρ fully satisfies the properties of a density operator, *i.e.*, (i) hermiticity, (ii) unit trace, and (iii) positive semidefiniteness. Finally, we calculate the entropy from this density matrix via Eq. (2).

of a Hermitian matrix with non-negative eigenvalues and with unit trace was solved almost a century ago by John von Neumann [25] and Lev Landau [26]. However, a form of entropy defined in terms of a density operator had not been applied to Pearson correlation matrices until now. This procedure will thereby allow the calculation of the entropy from the Pearson matrix (see Fig. 1).

Direct estimation of entropy from the Pearson matrix. – We first review the definition of the Pearson correlation matrix. Consider N data sets, each with a population of n measurements. Let $\mathbf{x}_i = (x_i^{(1)}, \dots, x_i^{(n)})$ denote the sequence of n measurements of the i -th data set. Let $\langle \cdot \rangle$ denote the average taken over the population of n points, so that $\mathbf{X}_i = \mathbf{x}_i - \langle \mathbf{x}_i \rangle$ represents deviations from the mean $\langle \mathbf{x}_i \rangle$ and $\sigma_i^2 = \langle \mathbf{X}_i^2 \rangle$ is the variance of \mathbf{x}_i . The correlation between the i -th and j -th data sets is then given by the Pearson correlation coefficient

$$R_{ij} = \frac{1}{n} \sum_{k=1}^n \left[\frac{x_i^{(k)} - \langle \mathbf{x}_i \rangle}{\sigma_i} \right] \left[\frac{x_j^{(k)} - \langle \mathbf{x}_j \rangle}{\sigma_j} \right] = \frac{\langle \mathbf{X}_i \mathbf{X}_j \rangle}{\sigma_i \sigma_j}. \quad (3)$$

The Pearson correlation matrix is the $N \times N$ matrix \mathbf{R} with entries R_{ij} as in Eq. (3).

Given a Pearson correlation matrix \mathbf{R} , the entropy is often estimated by using a different (but related) object as a proxy, *viz.*, a binary adjacency matrix \mathbf{A} . The latter is defined by imposing a threshold value ξ over the entries of \mathbf{R} . Specifically, one sets $A_{ij} = 1$ whenever $|R_{ij}| \geq \xi$ for $i \neq j$, and $A_{ij} = 0$ otherwise [27]. The matrix \mathbf{A} defines a graph with N nodes and undirected and unweighted edges. The entropy estimation, then, becomes a matter of computing the Shannon entropy of certain probability distributions embedded in the graph structure of \mathbf{A} , as explained earlier. We note that, in network analysis,

the entropy in Eq. (2) has previously been used with adjacency matrices [28, 29] and networks in general [30], rendering a properly sub-additive spectral entropy for model selection of complex networks [3, 31, 32]. It has also been analyzed in the context of measures of fit of multiple latent variables [33]. However, it has never been applied directly to Pearson correlation matrices.

Numerous properties of correlation matrices can be extracted from their thresholded counterparts, partly due to the information that remains stored in the topology of simple graphs [34]. Hence, these methods have become pivotal and ubiquitous in the study of complex systems [13–15]. In neuroscience, for instance, different thresholding schemes are extensively used to deduce the structural and functional connectivity of the brain, despite the selected method possibly influencing over and misleading the neuroimaging data analysis [35, 36] (for context, see a thorough review of thresholding in network neuroscience [37, 38]). But there are yet other drawbacks to this approach, in addition to the limitations previously mentioned [17–20]. Not only can thresholding lead to loss of information, it can even inject spurious complexity into genuinely random networks [39]. For these reasons, such methods require caution when applied to real-world networks [9].

In order to overcome these difficulties, we develop a way to estimate the entropy directly from the Pearson correlation matrix, without relying on an adjacency matrix. Our method rests on the following mathematical foundation: if \mathbf{R} is an arbitrary $N \times N$ Pearson correlation matrix, then

$$\rho = \frac{\mathbf{R}}{N} \quad (4)$$

satisfies all the conditions for a density operator, namely, (i) hermiticity, (ii) unit trace, and (iii) positive

semidefiniteness. To see this, observe that \mathbf{R} has real and symmetric entries, from which follows claim (i). Next, the diagonal entries are given by

$$R_{ii} = \frac{\langle \mathbf{X}_i^2 \rangle}{\sigma_i^2} = 1, \quad (5)$$

so that $\text{tr} \mathbf{R} = N$, leading to claim (ii). For (iii), it suffices to show that \mathbf{R} is positive semidefinite. In other words, we must show that $\mathbf{v} \cdot \mathbf{R} \mathbf{v} \geq 0$ for all $\mathbf{v} \in \mathbb{R}^N$. In fact, the positive semidefiniteness of Pearson correlation matrices is well known. Observe that

$$\sum_{ij} v_i \left(\sum_k X_i^{(k)} X_j^{(k)} \right) v_j = \sum_k \left| \sum_i v_i X_i^{(k)} \right|^2 \geq 0. \quad (6)$$

We can now state our main result. Given an arbitrary Pearson correlation matrix, the entropy can be calculated from Eq. (2), with ρ given by Eq. (4). We remark in passing that many other correlation matrices (*e.g.*, Spearman, Kendall) will satisfy analogous conditions, so long as they consist of real symmetric entries [40]. For normalized time series this definition of the density operator is the same as the covariance matrix divided by its trace. Furthermore, one can readily verify that $S(\rho) = \log N$ is the maximal entropy value for a system of N uncorrelated data sets.

In conceptual terms, the method here proposed is a mathematical device that yields a set of scaled eigenvalues, in such a way that makes it possible to assign a well defined entropy to any given Pearson correlation matrix. This entropy is the analog of the von Neumann entropy for a density operator ρ and is a continuous non-negative real functional of the Pearson matrix. However, apart from the special case where ρ would correspond to a pure state in quantum mechanics, the matrix $\rho = \mathbf{R}/N$ corresponds to a mixed state in quantum statistical mechanics, such that it encodes classical probabilities that are precisely the eigenvalues of the scaled Pearson correlation matrix.

Since probability distributions (and density operators) become coarse-grained (hence effectively renormalized) in the presence of noise, the entropy of two different data sets with similar levels of added noise can still be usefully compared. Therefore, this is an advantage of our method given that it is robust to the addition of noise. Moreover, although the Pearson coefficient is a pair correlation coefficient, it is still sensitive to nonlinear effects because it is the expected value of a bilinear quantity.

It is worth pointing out a crucial difference between the method proposed here and the other thresholding-based methods of calculating entropy. Whereas the proposed entropy is a continuous function (functional) of the Pearson matrix, the usual thresholding-based entropies are discontinuous. To see this, recall that the Heaviside

step function is defined as

$$\Theta(x) = \begin{cases} 0, & x \leq 0 \\ 1, & x > 0 \end{cases}. \quad (7)$$

This function has a discontinuity at $x = 0$, so that any entropy calculated via thresholding is necessarily a discontinuous function of the Pearson matrix, due to the explicit or implicit use of the Heaviside step function to perform thresholding. In contrast, the proposed entropy is a continuous functional of the Pearson matrix.

We thus have a robust and direct approach to obtain the entropy of correlation matrices. Crucially, at no point have we introduced *a priori* estimates, hence the resulting entropy is free from arbitrary or extraneous assumptions (*e.g.*, choice of threshold ξ). Of course, one can additionally use thresholding to obtain a suitable \mathbf{A} , but even then our protocol can still be useful. For example, it can be used to obtain an exact expression for the entropy of an idealized ranked set of correlated data. Such results might then yield a null hypothesis for subsequent statistical inference or undertake more rigorous hypothesis testing.

In what follows, we apply our main result to illustrative examples that are easy to understand, in order to further build intuition on the subject. We then apply our method to functional magnetic resonance imaging (fMRI) time series of the human brain activity. We also have included an extra material where we discuss in some detail the related topic of Guttman-scalable Pearson matrices for those readers interested in further applications (see the [Supplementary Material](#)).

Examples of some Pearson matrices. – Consider first the scenario of N series where all \mathbf{x}_i and \mathbf{x}_j are statistically independent, *i.e.*, uncorrelated: $\langle \mathbf{X}_i \mathbf{X}_j \rangle = \langle \mathbf{X}_i^2 \rangle \delta_{ij}$. Thus from equation Eq. (3), $R_{ij} = \delta_{ij}$, and, as expected, the density operator admits the (completely mixed state) representation $\rho = \mathbf{I}/N$, where \mathbf{I} is the $N \times N$ identity matrix. From Eq. (2) one immediately finds that $S = \log N$. It is a simple exercise to show that this is the maximum possible entropy for an $N \times N$ density matrix.

Compare the above with the other extreme, *i.e.*, when all pairs are perfectly autocorrelated, so that $\mathbf{X}_i/\sigma_i = \mathbf{X}_j/\sigma_j$ for all i, j . Then, clearly, $R_{ij} = 1$, so that $\mathbf{R}^2 = N\mathbf{R}$. The matrix ρ is thus idempotent: $\rho^2 = \rho$. It follows immediately that

$$\text{tr}(\rho \log \rho) = \text{tr}(\rho \log \rho^2) = 2\text{tr}(\rho \log \rho), \quad (8)$$

hence $\text{tr}(\rho \log \rho) = 0$. Then we have that $S = 0$, which is the absolute minimum possible value (corresponding to a pure state configuration). Note that, in contrast to statistical moments, the entropy is not strongly dependent on the tails of the distribution of eigenvalues, since $\lambda_j \log \lambda_j \rightarrow 0$ in the limit $\lambda_j \rightarrow 0$.

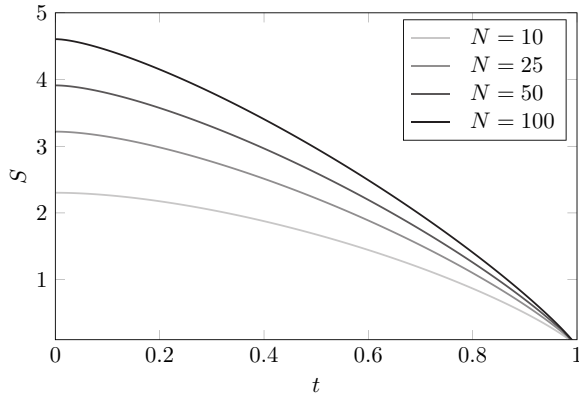


Figure 2. Entropy S as a function of the parameter t for the example given by Eq. (9). The case $t = 1$ represents maximal correlation ($S = 0$) while $t = 0$ represents uncorrelated series, leading to maximum entropy. $S = \log N = \log 100 \approx 4.6$, as expected.

Let us now focus on analytically solvable examples, in order to illustrate better how the entropy depends on the entries of the Pearson matrix. Consider thus the following situation which is an interpolation between the cases of maximum and minimum entropies.

Let the Pearson matrix now be given according to

$$R_{ij}(t) = t + \delta_{ij}(1 - t). \quad (9)$$

This corresponds to a situation where any pair of distinct series have autocorrelation $t \in [-1, 1]$. It is easy to check that the density operator $\rho(t) = \mathbf{R}(t)/N$ for this Pearson matrix is well behaved. $N - 1$ of the N eigenvalues — all but one of them — are identically equal to $(1 - t)/N$. The last remaining eigenvalue equals $(1 + (N - 1)t)/N$. The entropy is thus

$$S(t) = \log N - \frac{N-1}{N}(1-t) \log(1-t) - \frac{1}{N}[1 + (N-1)t] \log[1 + (N-1)t]. \quad (10)$$

The special case $t = 0$ recovers the maximum entropy $S = \log N$ while $t = 1$ recovers the minimum entropy $S = 0$. Figure 2 shows how the entropy varies with t in between the two limiting cases for $N = 100$.

Our final example is the case of a modular Pearson matrix \mathbf{R}_M representing 2 weakly correlated sets of N strongly correlated series. Let the strong correlation be t and let the weak correlation be ϵ . Such a Pearson matrix is a $2N \times 2N$ matrix with a 2×2 block structure:

$$\mathbf{R}_M(t, \epsilon) = \begin{bmatrix} \mathbf{R}(t) & \epsilon \\ \epsilon & \mathbf{R}(t) \end{bmatrix}. \quad (11)$$

where the $\mathbf{R}(t)$ are given by Eq. (9) and the matrix ϵ has every entry equal to ϵ . In this case, all but 2 of the eigenvalues of the corresponding density matrix $\rho(t, \epsilon)$

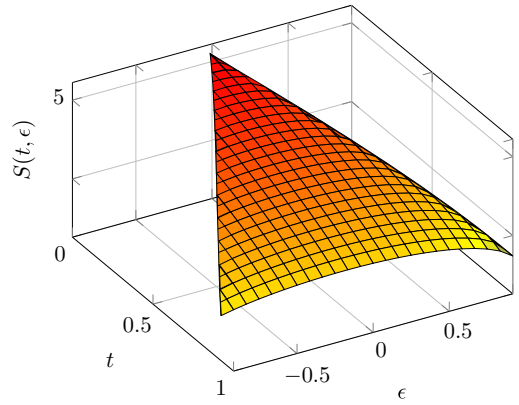


Figure 3. Entropy S as a function of the parameter t and ϵ for the “modular” example given by Eq. (11) for $N = 100$.

are identically equal to $(1 - t)/(2N)$. The remaining 2 eigenvalues are $(1 + (N - 1)t \pm N\epsilon)/(2N)$. Hence, the entropy is immediately obtained:

$$S(t, \epsilon) = \frac{1}{2N} \left[-(\epsilon N + (N - 1)t + 1) \log \left(\frac{\epsilon N + (N - 1)t + 1}{2N} \right) + (\epsilon N - Nt + t - 1) \log \left(\frac{-\epsilon N + (N - 1)t + 1}{2N} \right) + 2(N - 1)(t - 1) \log \left(\frac{1 - t}{2N} \right) \right]. \quad (12)$$

Note that for the condition of positive semidefiniteness to be satisfied, we require $1 + (N - 1)t \pm N\epsilon \geq 0$, so that for fixed t we must have

$$|\epsilon| \leq \frac{1 + (N - 1)t}{N}. \quad (13)$$

Figure 3 shows the entropy as a function of t and ϵ for $N = 100$. For fixed t , a smaller ϵ leads to higher entropy. For $\epsilon = 0$ the 2 modules become independent and the entropy is maximized.

Application to a real-world data set. — What about Pearson matrices with entropy in between the maximum and minimum entropies? This scenario is, of course, the case of crucial interest for analyzing empirical data. As a practical demonstration of the method’s power and its potential applicability, we calculate the entropy of Pearson correlation matrices obtained from fMRI time courses of the human brain. Specifically, we assess the hypothesis that brain signals display an increase of entropy while under the influence of a psychedelic [41]. For this purpose, we chose the indigenous beverage ayahuasca [42], a decoction with rapid antidepressant effects partially mediated by the serotonergic agonist N,N -dimethyltryptamine (DMT) [43].

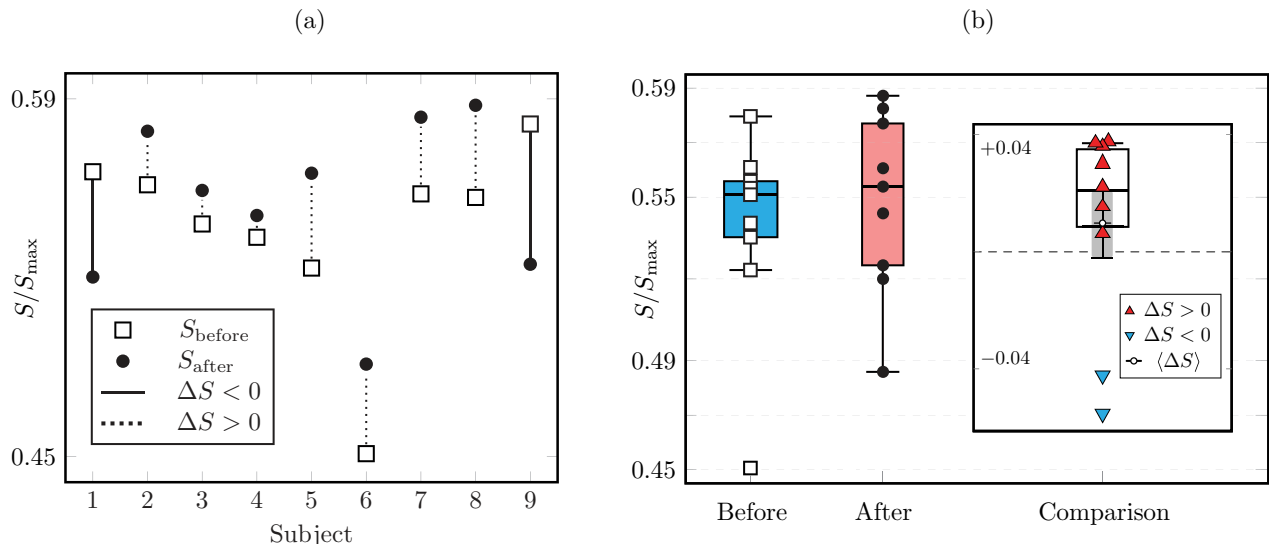


Figure 4. Entropy before and after ayahuasca. (a) The plot shows the entropy S of the nine subjects (horizontal axis), both before (S_{before}) and after (S_{after}) ayahuasca ingestion, normalized by $S_{\text{max}} = \log(104)$. Entropy variation $\Delta S = S_{\text{after}} - S_{\text{before}}$ was found positive for seven subjects (dotted lines). (b) Box plots of the distribution S_{before} and S_{after} , with the single outlier being Subject 6 in the condition prior to ayahuasca consumption. On the right, the inset shows the box plot of the distribution of entropy variation. The error bar of the average $\langle \Delta S \rangle$ taken over all nine subjects is represented by the shaded region, and only slightly touches the $\Delta S < 0$ zone. These findings are broadly consistent with the hypothesis of psychedelic-induced brain entropy increase, although one must be careful due to the small number of subjects involved.

A total of nine healthy human volunteers were assigned to a neuroimaging session both before and after ayahuasca intake. We obtained a set of $N = 104$ fMRI time series of the blood-oxygen-level-dependent (BOLD) signal of the human brain from each subject at both conditions. We next calculated the density operators. The 18 correlation matrices were individually scaled according to Eq. 4 using $N = 104$. For a detailed description of the acquisition, preprocessing, and availability of the data, please refer to the [Supplementary Material](#).

In Fig. 4 we show the normalized entropy of all 18 matrices ρ , grouped in terms of subjects (from 1 to 9) for both experimental conditions (before and after ayahuasca ingestion). With the exception of two individuals (Subjects 1 and 9), we find positive entropy variation $\Delta S \equiv S_{\text{after}} - S_{\text{before}}$ among subjects (dotted lines). Although the low number of individuals demands careful analysis in regards to statistical significance, our findings are in agreement with previous measures of increased brain entropy due to a psychedelic ingestion [21–23, 44, 45]. Ours, however, crucially avoids the need of thresholding schemes. Finally, measures of brain entropy might differ in the literature, for instance, by probing either static or dynamical properties of network links [46, 47]. Here, the entropy proposed is a measure of the network connectivity repertoire, thus an entropy of the links.

In summary, we have proposed an entirely objective

procedure for directly estimating a unique entropy of a general Pearson matrix without needing to use thresholding. We hope that our results will contribute positively to satisfy, at least partially, the growing and urgent demand in diverse fields of science for a reliable method of estimating the information entropy associated with correlations.

A.V. thanks the support of Progetti di Ricerca di Interesse Nazionale (PRIN) grant 20174TPEFJ “TRIPS”. This work was supported by the Brazilian agencies Conselho Nacional de Desenvolvimento Científico e Tecnológico (CNPq) (Grants No. 304532/2019-3, No. 305062/2017-4, and No. 302051/2018-0) Coordenação de Aperfeiçoamento de Pessoal de Nível Superior (CAPES), and Fundação de Amparo à Ciência e Tecnologia do Estado de Pernambuco (FACEPE).

-
- [1] Albert, R. and Barabási, A. *Rev. Mod. Phys.* **74**, 47 (2002).
 - [2] Anand, K. and Bianconi, G. *Phys. Rev. E* **80**, 045102(R) (2009).
 - [3] De Domenico, M. and Biamonte, J. *Phys. Rev. X* **6**, 041062 (2016).
 - [4] Almog, A. and Shmueli, E. *Sci. Rep.* **9** 10832 (2019).
 - [5] Chakraborti, A. *et al. J. Phys. Complex.* **2**, 015002 (2021).
 - [6] Gómez-Gardeñes, J. and Latora, V. *Phys. Rev. E* **78**,

- 065102(R) (2008).
- [7] Bullmore, E. and Sporns, O. *Nat. Rev. Neurosci.* **10**, 186–198 (2009).
- [8] Santos, F. A. N. *et al. Phys. Rev. E* **100**, 032414 (2019).
- [9] Nicolini, C. *et al. Neuroimage* **211**, 116603 (2020).
- [10] Shannon, C. *Bell System Tech. J.* **27**, 623-656 (1948).
- [11] Latora, V. and Marchiori, M. *Phys. Rev. Lett.* **87**, 198701 (2001).
- [12] Yan, X. *et al. Phys. Rev. E* **98**, 042304 (2018).
- [13] Kumar, S. and Deo, N. *Phys. Rev. E* **86**, 026101 (2012).
- [14] Eguíluz, V. M. *et al. Phys. Rev. Lett.* **94**, 018102 (2005).
- [15] Bassett, D. S. and Bullmore, E. *The Neuroscientist* **12**, 512-523 (2006).
- [16] Gallos, L. K., Makse, H. A. and Sigman, M. *PNAS* **109**, 2825-2830 (2012).
- [17] Rubinov, M. and Sporns, O. *Neuroimage* **56**, 2068-2079 (2011).
- [18] Kukreti, V. *et al. Front. Phys.* **8**, 323 (2020).
- [19] Langer, N., Pedroni, A. and Jäncke, L. *PLoS One* **8**, 1–9 (2013).
- [20] Garrison, K. A. *et al. Neuroimage* **118**, 651-661 (2015).
- [21] Tagliazucchi, E. *et al. Hum. Brain. Mapp.* **35**, 5442–5456 (2014).
- [22] Viol, A. *et al. Sci. Rep.* **7**, 7388 (2017).
- [23] Viol, A. *et al. Entropy* **21**, 128 (2019).
- [24] Ohya, M. and Petz, D. *Quantum Entropy and Its Use* (Springer-Verlag, 1993).
- [25] Von Neumann, J. *Nachr. Ges. Wiss. Göttingen*, 273 (1927).
- [26] Landau L. Z. *Phys.* **45**, 430 (1927).
- [27] Liu, Y. *et al. Brain* **131**, 945–961 (2008).
- [28] Passerini, F. and Severini, S. *Int. J. Agent Tech. Syst.* **1** 58-67 (2009).
- [29] Estrada, E., De la Pëna, J. A. and Hatano, N. *Linear Algebra Appl.* **443**, 235-244 (2014).
- [30] De Domenico, M. *et al. Phys. Rev. X* **3**, 041022 (2013).
- [31] De Domenico, M. *et al. Nat. Commun.* **6**, 6864 (2015).
- [32] Ghavasieh A. and De Domenico M. *Phys. Rev. Res.* **2**, 013155 (2020).
- [33] Golino H. *et al. Multivariate Behav. Res.* **56**, 874 (2021).
- [34] Viol, A., Vuksanović, V. and Hövel, P. *Physica A* **561**, 125233 (2021).
- [35] Van Wijk B. C. M. *et al. PLoS One* **5**, e13701 (2010).
- [36] Drakesmith M. *et al. Neuroimage* **118**, 313 (2015).
- [37] Hallquist M. N. and Hillary F. G. *Netw. Neurosci.* **3**, 1 (2018).
- [38] Fornito A. *et al. Fundamentals of brain network analysis* (Academic Press, 2016).
- [39] Cantwell, G. T. *et al. Phys. Rev. E* **101**, 062302 (2020).
- [40] Boudt, K., Cornelissen, J. and Croux, C. *Stat. Comput.* **22**, 471 (2012).
- [41] Carhart-Harris, R. L. *et al. Front. Hum. Neurosci.* **8**, 20 (2014).
- [42] Riba, J. *et al. J. Pharmacol. Exp. Ther.* **306**, 73-83 (2003).
- [43] Palhano-Fontes, F. *et al. Psychol. Med.* **49**, 655-663 (2019).
- [44] Lebedev, A. V. *et al. Hum. Brain. Mapp.* **37**, 3203–3213 (2016).
- [45] Schartner, M. M. *Sci. Rep.* **7**, 46421 (2017).
- [46] Keshmiri, S. *Entropy* **22**, 917 (2020).
- [47] McCulloch E. D. *et al. Neurosci. Biobehav. Rev.* **128**, 104689 (2022).

Supplementary Material

Guttman Scaling

The entropy for the homogeneous Guttman-scalable Pearson matrix

Whenever a new method of data analysis is developed, it is always useful to obtain exact analytical results from it, thus aiming to gain proper insights on the characteristics of the approach. An idealized, but useful, type of correlated data is that of a perfect Guttman scale [1, 2]. It has been used to study data in many different areas of knowledge. But in particular, it finds important usages in health and biomedical related problems [3–7]. We thus shall address a set of correlated data following the Guttman scaling.

In the homogeneous case [8] (see below), many exact results are known for the corresponding Pearson correlation matrix \mathbf{R}_{hG} [8, 9]. As we will show, this allows to write an analytical expression for the entropy S_{hG} of \mathbf{R}_{hG} . Although real data rarely fits in with a perfect Guttman scale, the present S_{hG} could play the role of a null hypothesis model [8]. Indeed, it may be useful for testing hierarchies as well as features of correlations in distinct processes involving N populations [10, 11]; in our case all with the same size n and described by ($i = 1, \dots, N$)

$$\mathbf{x}_i = (x_i^{(1)}, \dots, x_i^{(n)}) . \quad (\text{S1})$$

Moreover, Guttman scaling is a very instructive example of how the entropy portrays data with strong but not absolute correlations.

For our purposes, we concentrate on dichotomous or binary *events* (or “items”, a more common terminology in the area of statistical measurement theory [8, 12, 13]). Thus, to each properly defined event i we can associate two distinct numerical values, 0 and 1. For a given instance or realization pattern for the collection of events, the numerical value 1 (0) for the event i means it has (has not) taken place in that pattern.

The idea underlying the Guttman scaling, also known as cumulative scaling or scalogram analysis, is to be able to create a table or indicator matrix — which should not be confused with the correlation matrix \mathbf{R} itself — assembling the data in a very particular manner. If such construction is possible for the data set, the indicator matrix would display a triangular structure, with all entries in the lower (upper) part equal to 1 (0), see Table S1. Hence, within a given pattern of outcomes, there is a priority of events. If the event i has occurred, then event $i - 1$ has also occurred. The Table S1 explains in more detail the data organization.

Two extra assumptions for data already observing the Guttman arrangement are known as homogeneity conditions [8]. They can be stated as the following. (a) There is no full correlation between any two populations $\mathbf{x}_{i''}$ and $\mathbf{x}_{i'}$. Actually, in many contexts this is not a really restrictive hypothesis, either because such coincidence is rare or, if it is not, for N large enough we can just eliminate the akin \mathbf{x}_i from the data set without losing relevant statistical significance. (b) The probability of obtaining the different patterns of outcomes indicated in Table S1 are the same, *i.e.*, the \mathcal{N}_i in Table S1 are essentially all equal. Arguably, this may seem a too restricting imposition [9]. But perhaps a bit surprising, it has been verified numerically that certain results (like principal component analysis and certain properties of covariance matrices) for homogeneous data do not depart very much from the case where the \mathcal{N}_i display a normal distribution (provided the populations have ample variability [8, 9]).

Therefore, it is correct to affirm that data obeying the homogeneous Guttman scaling is not ubiquitous. But the relevant fact for our purposes is that, precisely because of that, the Pearson correlation matrix \mathbf{R}_{hG} can be derived analytically [8]. Furthermore, its exact eigenvalues $\tilde{\lambda}_i$ have been obtained in [8]. Since the eigenvalues λ_i of ρ_{hG} are simply $\tilde{\lambda}_i/N$, then from [8] we get

$$\lambda_i = \frac{1 + N^{-1}}{i(i+1)}. \quad (\text{S2})$$

Notice that the λ_i depend only on a single parameter, the population number N . So, finally we find

$$\begin{aligned} S_{hG} &= -(1 + N^{-1}) \sum_{i=1}^N \frac{1}{i(i+1)} \ln \left[\frac{1 + N^{-1}}{i(i+1)} \right] \\ &= \ln[N] - (1 - N^{-2}) \ln[N + 1] \\ &\quad + 2(1 + N^{-1}) \sum_{i=1}^{N-1} \frac{1}{i(i+2)} \ln[i + 1]. \end{aligned} \quad (\text{S3})$$

Since it is well known that the series $\sum_{i=1}^{\infty} \ln[i]/i^2$ converges, it is not difficult to prove that S_{hG} also converges as $N \rightarrow \infty$. Also, due to the peculiar way items are correlated in a homogeneous Guttman-scalable data collection, after a rapid increase with N , the entropy S_{hG} tends to a plateau as N increases. Figure S1 illustrates the general behavior of $S_{hG}(N)$, also comparing it with the entropy for a Pearson correlation matrix of a totally uncorrelated data set, for which $S = \ln[N]$.

Table S1. The data table (or indicator matrix) organized in a specific ordering of events i , with $i = 1, \dots, N$. Along each row — representing a particular configuration of events occurrence: a pattern — the entry 1 (0) means that the corresponding event has (has not) taken place. The depicted structure illustrates a perfect Guttman scaling: for the pattern i , only the events up to $i - 1$ do take place. This ascribes a ranking or degree of prevalence among the distinct events within a specific pattern. \mathcal{N}_i is the number of times the pattern i is found in the full data set collection.

Pattern	Event 1	Event 2	Event 3	Event 4	Event 5	...	Event N	Number of occurrences
1	0	0	0	0	0	...	0	\mathcal{N}_1
2	1	0	0	0	0	...	0	\mathcal{N}_2
3	1	1	0	0	0	...	0	\mathcal{N}_3
4	1	1	1	0	0	...	0	\mathcal{N}_4
5	1	1	1	1	0	...	0	\mathcal{N}_5
6	1	1	1	1	1	...	0	\mathcal{N}_6
\vdots	\vdots	\vdots	\vdots	\vdots	\vdots	\vdots	0	\vdots
$N + 1$	1	1	1	1	1	...	1	\mathcal{N}_{N+1}

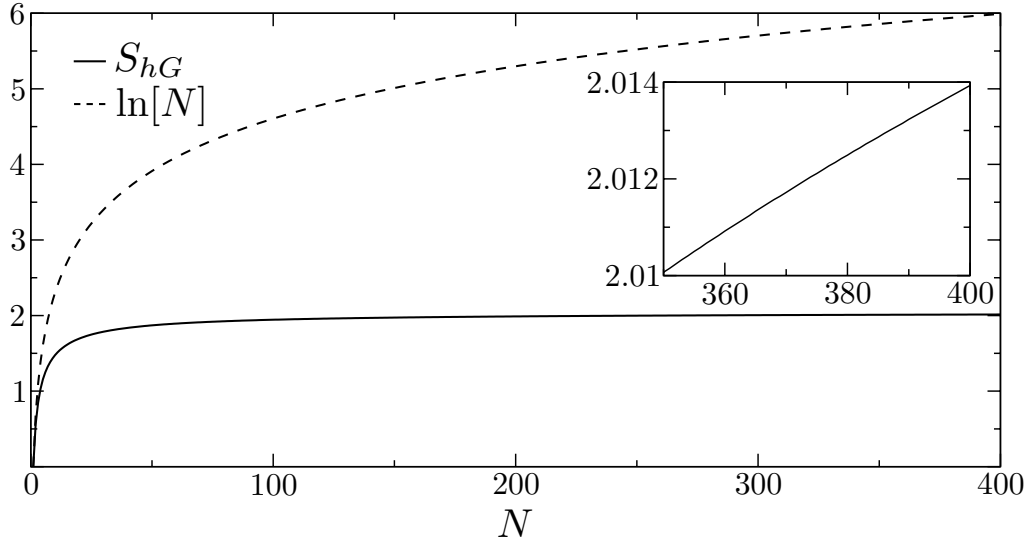


Fig. S1. The entropy for a Pearson correlation matrix resulting from an ideal homogeneous Guttman-scalable data set. The entropy S_{hG} tends to a constant value for the population (number of items) N going to infinity (see the inset). For comparison, it also shows the entropy for a completely uncorrelated data set, for which $S = \ln[N]$.

Possible ways to frame a general data set in terms of “events”

An important question is certainly how a given data set, given as in Eq. (S1), can be described in terms of events and thus to allow an indicator matrix representation. Below we summarize two possible procedures to do so.

The first is when we can associate phenomenological behavior to the data. Then, we can define an event by classifying *appropriate* (*i.e.*, easier to characterize in terms of ranking of predominance) information which can be inferred once we know the explicit values of the $x_i^{(j)}$. For example, suppose whenever $x_i^{(j)}$ is above a threshold γ , we can conclude it has been a high electrical pulse crossing the population i at the measurement step j . Then, an event could be the existence (1) or not (0) of an intense pulse. Further, suppose that a determined biochemical reaction takes place when $\alpha < x_i^{(j)} < \beta$. Such reaction could also constitute another event, with the values 0 and 1 being ascribed conforming to the numerical intervals for the $x_i^{(j)}$. Importantly, if $\langle x_i \rangle < \gamma < \alpha$, in principle we may expect an order of priority between the high pulse and the biochemical reaction. In this way, we might try to organize the events as in Table S1 according to the numerical sequences in Eq. (S1). Of course, such an approach is heavily based on the concrete understanding of the physical, chemical, biological, etc., aspects underlying the problem studied. In the absence of this type of knowledge, the protocol is not feasible.

A second possibility is to consider an algorithmically oriented method, not relying on any *a priori* qualitative information about the process. But then, admittedly it has a higher chance of not satisfying the perfect homogeneous Guttman scaling [9, 14]. For the full data set, let us define a and b as the minimum and maximum values assumed by the entire collection of $x_i^{(j)}$. Thus, we divide $[a, b]$ into $N + 1$ intervals $\Delta_0, \Delta_1, \dots, \Delta_N$. Here, Δ_0 must represent the most frequent numerical interval for the data set, with the other Δ_i presenting a decreasing order of occurrence with i . The events to be considered in the indicator matrix are the occurrence of the intervals $\Delta_1, \Delta_2, \dots, \Delta_N$ (Δ_0 is not explicitly included in the events table, but it contributes with the “0”’s in it). For M_i the number of times the interval Δ_i appears in the data set, we have $\sum_{i=0}^N M_i = n \times N$. All the incidences M_i ($i = 0, 1, \dots, N$) of the events Δ_i should thus be combined to generate a structure like that in Table S1. An illustration of how to proceed in the particular case the data allows an exact homogeneous Guttman scaling is depicted in Table S2. Finally, given that there is a certain freedom in choosing the intervals Δ_i , this must be done in such way to get an indicator matrix as close as possible to the pattern in Table S1.

Table S2. Consider that for a data set of $N = 3$ and $n = 4$, the twelve $x_i^{(j)}$ assume $M_0 = 6$, $M_1 = 3$, $M_2 = 2$, $M_3 = 1$ values, respectively, in the numerical intervals Δ_0 , Δ_1 , Δ_2 and Δ_3 . Then, taking as the events the instances (irrespective of i and j) in which the variables are within Δ_1 , Δ_2 and Δ_3 , one can construct an indicator matrix exactly satisfying a homogeneous Guttman scaling. Indeed, the three, two and one “1”’s in the columns Event 1, Event 2 and Event 3, correspond to M_1 , M_2 and M_3 , whereas the total of six “0”’s spread in the whole table are due to M_0 .

Pattern	Event 1: Interval Δ_1	Event 2: Interval Δ_2	Event 3: Interval Δ_3	Occurrence of the pattern
1	0	0	0	1
2	1	0	0	1
3	1	1	0	1
4	1	1	1	1

METHODS

Data acquisition

A total of nine healthy adults (five women) with no history of neurological or psychiatric disorders (assessed by DSM-IV structured interview), volunteered to ingest 120–200 mL (2.2 mL/kg of body weight) of ayahuasca known to contain 0.8 mg/mL of its main psychoactive compound DMT and 0.21 mg/mL of harmine, a β -carboline which allows for the entrance of DMT into the bloodstream [15]. The volunteers were assigned with two task-free fMRI sessions: the first one prior to the ayahuasca ingestion, and the second one at 40 minutes after the brew intake (when ayahuasca’s effects begin to occur, lasting for approximately four hours). Both sessions required the participants to maintain an awake resting state. The experimental procedure was approved by the Ethics and Research Committee of the University of São Paulo at Ribeirão Preto (No. 14672/2006). Written informed consent was obtained from all volunteers. All experimental procedures were performed in accordance with the relevant guidelines and regulations.

The fMRI images were acquired in a 1.5 T scanner (Siemens, Magnetom Vision), using an EPI-BOLD sequence to obtain 150 volumes with parameters TR = 1700 ms, TE = 66 ms, FOV = 220 mm, matrix 64×64 , and voxel dimensions of $1.72 \text{ mm} \times 1.72 \text{ mm} \times 1.72 \text{ mm}$. The images were preprocessed in the FSL software [16], and consisted of slice-timing, head motion, and spatial smoothing corrections (Gaussian kernel, FWHM = 5 mm). Nine regressors were used within a general linear model (GLM): six regressors to movement correction; one to white matter signal; one to cerebrospinal fluid; and one to global signal. The images were normalized to the standard anatomical space of the Montreal Neurological Institute (MNI152 template) [17].

The preprocessed fMRI images were then parcellated into 110 anatomical regions of interest (ROIs) in accordance with the Harvard-Oxford cortical and subcortical atlas (see Supplementary Table S3). Due to acquisition limitations, six regions were excluded from further analysis. Thus, for each one of the remaining 104 ROIs, we averaged the BOLD signal of the regions’ associated voxels, resulting in time courses listing a sequence of $n = 150$ data points. To reduce confounders in the signal, a maximum overlap discrete wavelet transform (MODWT) was applied to the series in order to select the typical frequency range (0.01–0.1 Hz) of the resting state signal [18]. Finally, in possession of the $N = 104$ time series \mathbf{x}_i , we pairwise-correlated them using the Pearson correlation coefficient of equation 3, resulting in the 104×104 Pearson correlation matrix \mathbf{R} . We thus ended up with a total of 18 functional connectivity networks: two conditions (before and after ayahuasca) for each of the nine subjects involved.

Subjective evaluation

Individual responses of the Clinician-Administered Dissociative States Scale (CADSS), a psychometric scale that can discriminate subjects with dissociative disorders [19], were collected and their scores were plotted against the respective entropy. All subjects showed an increase in depersonalization as assessed by the CADSS scale (see Supplementary Figure S2).

DATA AVAILABILITY

The datasets generated and/or analysed during the current study are available in the GitHub repository, <https://github.com/hfelippe/arXiv.2106.05379>. In-house scripts to generate the correlation matrices and figures

are also available in the referred repository. The original fMRI data can be sent upon request to DBA (draulio@neuro.ufrn.br).

-
- [1] Guttman, L. The quantification of a class of attributes: a theory and method of scale construction. in *The prediction of personal adjustment*, (eds. P. Horst et al.) 319-348 (Social Science Research Council, New York, 1941).
- [2] Guttman, L. The principal components of scale analysis. in *Measurement and prediction*, (eds. S. A. Stouffer et al.) 312-361 (Princeton University Press, Princeton, 1950).
- [3] Davies, R. G. *Computer Programming in Quantitative Biology* (Academic Press, London, 1971).
- [4] Tractenberg, R. E., Yumoto, F., Aisen, P. S., Kaye, J. A. & Mislevy, R. J. Using the Guttman scale to define and estimate measurement error in items over time: the case of cognitive decline and the meaning of “Points Lost”. *PLoS One* **7**, e30019 (2012).
- [5] Argyle, M. *The Scientific Study of Social Behaviour* (Routledge, New York, 2013).
- [6] Maggino, F. Guttman Scale. in *Encyclopedia of Quality of Life and Well-Being Research*, (ed. A. C. Michalos) 2626-2630 (Springer, Dordrecht, 2014).
- [7] Warrian, K. & Spaeth, G. Health-related quality of life measures in the information age. in *Handbook of Research on Information Technology Management and Clinical Data Administration in Healthcare*, (ed. A. Dwivedi) 725-745 (Medical Information Science Reference, Hershey, 2009).
- [8] Zwick, R. Some properties of the Pearson Correlation Matrix of Guttman-Scalable Items. *ETS Research Report Series* **1986**, i-23 (1986).
- [9] Davis-Stober, C. P., Doignon, J.-P. & Suck, R. A Note on the Eigensystem of the Covariance Matrix of Dichotomous Guttman Items. *Front. Psychol.* **6**, 1767 (2015).
- [10] Kendall, M. *Rank Correlation Methods*, 5th ed. (Oxford University Press, 1990).
- [11] Piao, L. & Fu, Z. Quantifying distinct associations on different temporal scales: comparison of DCCA and Pearson methods. *Sci. Rep.* **6**, 36759 (2016).
- [12] Goodman, L. A. A New Model for Scaling Response Patterns: An Application of the Quasi-Independence Concept. *J. Am. Stat. Assoc.* **70**, 755-768 (1975).
- [13] Hand, D. J. Statistics and the Theory of Measurement. *J. R. Statist. Soc. A* **159**, 445-492 (1996).
- [14] Coombs, C. H., Coombs, L. C. & Lingo, J. C. Stochastic cumulative scales in *Theory construction and data analysis in the behavioral sciences*, (ed. S. Shye) 280–298 (Jossey-Bass, San Francisco, 1978).
- [15] De Araujo, D. B. *et al.* Seeing with the eyes shut: neural basis of enhanced imagery following ayahuasca ingestion. *Hum. Brain Mapp.* **33**, 2550–2560 (2012).
- [16] Jenkinson, M., Beckmann, C. F., Behrens, T. E., Woolrich, M. W. & Smith, S. M. FSL. *Neuroimage* **62** 782-790 (2012).
- [17] Brett, M., Johnsrude, I. S. & Owen, A. M. The problem of functional localization in the human brain. *Nat. Rev. Neurosci.* **3**, 243–249 (2002).
- [18] Onias, H. *et al.* Brain complex network analysis by means of resting state fMRI and graph analysis: Will it be helpful in clinical epilepsy?. *Epilepsy Behav.* **38**, 71–80 (2014).
- [19] Bremner, J. D. *et al.* Measurement of dissociative states with the clinician-administered dissociative states scale (CADSS). *J. Trauma. Stress.* **11**, 125–136 (1998).

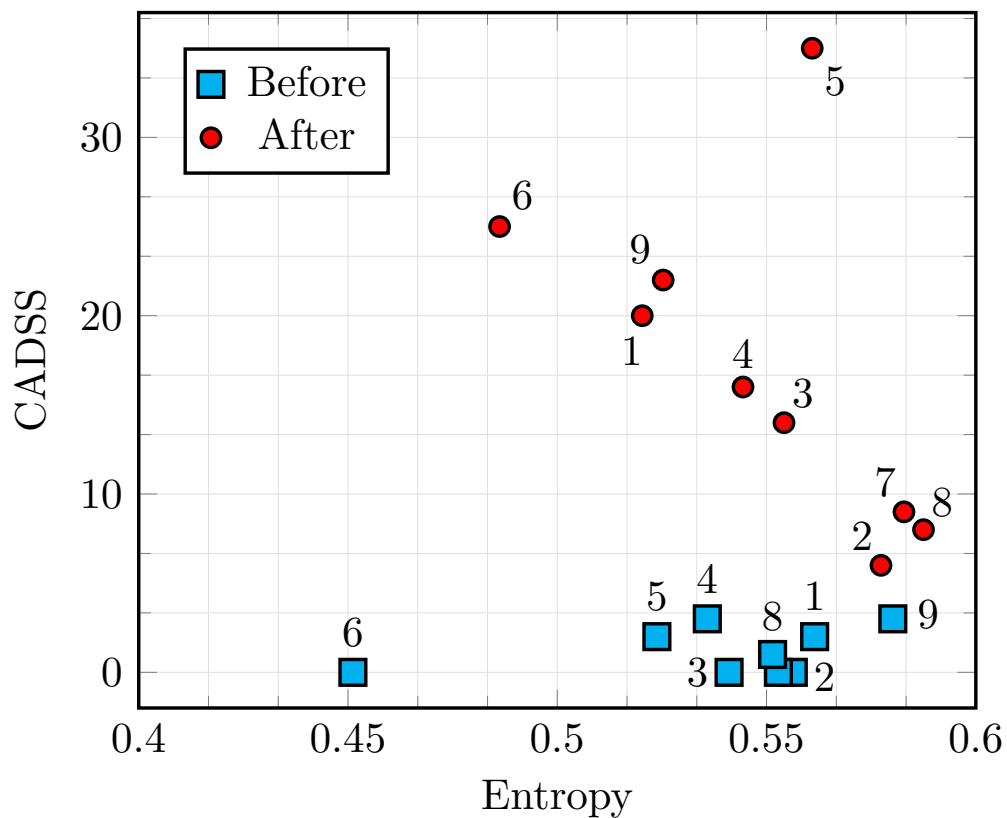


Figure S2. Entropy against CADSS scores. Blue squares refer to the condition prior to the ayahuasca ingestion, whereas red circles is posterior to the consumption of ayahuasca. The numbers 1 to 9 index the nine Subjects, respectively. We note that Subjects 1 and 9 were the only individuals who showed a decrease in entropy after ingestion of ayahuasca (a translation to the left on the graph). However, all subjects scored higher in the Clinician-Administered Dissociative States Scale (CADSS).

Table S3. Brain regions in accordance with the Harvard-Oxford cortical atlas. Asterisks (*) are assigned to the six excluded regions. Ordered pairs (i, j) refers to the left (i) and right (j) hemispheres of the corresponding region.

Index	Region
(1, 2)	Frontal Pole
(3, 4)	Insular Cortex
(5, 6)	Superior Frontal Gyrus
(7, 8)	Middle Frontal Gyrus
(9, 10)	Inferior Frontal Gyrus, pars triangularis
(11, 12)	Inferior Frontal Gyrus, pars opercularis
(13, 14)	Precentral Gyrus
(15, 16)	Temporal Pole
(17, 18)	Superior Temporal Gyrus, anterior division
(19, 20)	Superior Temporal Gyrus, posterior division
(21, 22)	Middle Temporal Gyrus, anterior division
(23, 24)	Middle Temporal Gyrus, posterior division
(25, 26)	Middle Temporal Gyrus, temporooccipital part
(27, 28)*	Inferior Temporal Gyrus, anterior division
(29, 30)	Inferior Temporal Gyrus, posterior division
(31, 32)	Inferior Temporal Gyrus, temporooccipital part
(33, 34)	Postcentral Gyrus
(35, 36)*	Superior Parietal Lobule
(37, 38)	Supramarginal Gyrus, anterior division
(39, 40)	Supramarginal Gyrus, posterior division
(41, 42)	Angular Gyrus
(43, 44)	Lateral Occipital Cortex, superior division
(45, 46)	Lateral Occipital Cortex, inferior division
(47, 48)	Intracalcarine Cortex
(49, 50)	Frontal Medial Cortex
(51, 52)	Juxtapositional lobule cortex
(53, 54)	Subcallosal Cortex
(55, 56)	Paracingulate Gyrus
(57, 58)	Cingulate Gyrus, anterior division
(59, 60)	Cingulate Gyrus, posterior division
(61, 62)	Precuneous Cortex
(63, 64)	Cuneal Cortex
(65, 66)	Frontal Orbital Cortex
(67, 68)	Parahippocampal Gyrus, anterior division
(69, 70)	Parahippocampal Gyrus, posterior division
(71, 72)	Lingual Gyrus
(73, 74)*	Temporal Fusiform Cortex, anterior division
(75, 76)	Temporal Fusiform Cortex, posterior division
(77, 78)	Temporal Occipital Fusiform Cortex
(79, 80)	Occipital Fusiform Gyrus
(81, 82)	Frontal Operculum Cortex
(83, 84)	Central Opercular Cortex
(85, 86)	Parietal Operculum Cortex
(87, 88)	Planum Polare
(89, 90)	Heschl's Gyrus (includes H1 and H2)
(91, 92)	Planum Temporale
(93, 94)	Supracalcarine Cortex
(95, 96)	Occipital Pole
(97, 104)	Thalamus
(98, 105)	Caudate
(99, 106)	Putamen
(100, 107)	Pallidum
(101, 108)	Hippocampus
(102, 109)	Amygdala
(103, 110)	Accumbens